NANO LETTERS

pubs.acs.org/NanoLett Letter

Plasmon-Enhanced Infrared Emission Approaching the Theoretical Limit of Radiative Cooling Ability

Rongkang Zhu, Dawei Hu, Zhi Chen, Xiaobao Xu, Yousheng Zou, Lin Wang,* and Yu Gu*

Cite This: *Nano Lett.* 2020, 20, 6974−6980 Read Online

ACCESS | Metrics & More | Article Recommendations | Supporting Information

ABSTRACT: Radiative cooling, a passive cooling technique, has shown great potentials in recent years to lower the power consumption of air conditioning. With the ever-increasing cooling power being reported, the theoretical cooling limit of such a technique is still unclear. In this work, we proposed a theoretical limit imposing an upper bound for the attainable cooling power. To approach this limit, we exploited the localized surface plasmon resonance (LSPR) of self-doped In_2O_3 nanoparticles, which enhance the emissivity in both primary and secondary atmospheric windows. The measured cooling power of poly(methyl methacrylate) (PMMA) films containing 4.5% In_2O_3 nanoparticles is very close to the limit with the closest value only about 0.4 W/m^2 below the limit. Hopefully, this work may help the researchers better evaluating the performance of their device in the future and pave the way for achieving even higher radiative cooling powers during the daytime operations with the help of LSPR.

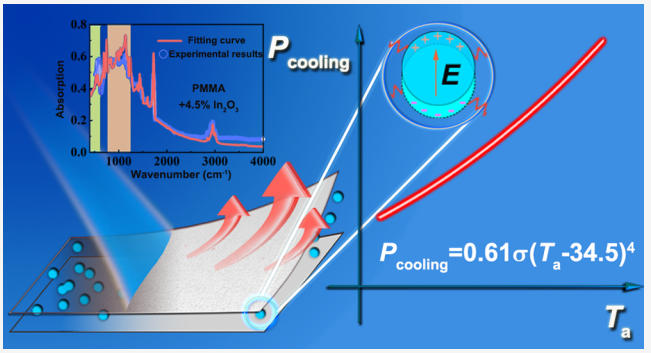

KEYWORDS: *radiative cooling, plasmon resonance, thermal emission, semiconductor nanoparticle, nanocomposites*

Traditional refrigeration technologies such as air conditioning consume power to achieve subambient temperatures. As previously reported, about 15% of the building's power consumption is attributed to air conditioning.[1] The ever-increasing power consumed by air conditioning has raised the global demand for energy and also brings about other environmental problems including the release of greenhouse gases. Radiative cooling, a passive cooling technique relying on radiating energy directly into the outer space, can work without any external energy input and has the potential to significantly lower the energy consumption.[2]

To achieve efficient radiative cooling, infrared emitters emitting strongly in the atmospheric window are necessary.[3−5] Two atmospheric windows are available in the mid-infrared range: the primary window of 8−13 μm and the secondary window of 16−28 μm. The primary window has a higher transmittance than the secondary window[4,6] and matches better with the peak of the blackbody radiation spectrum at room temperature (300 K) (Figure 1a). Even though an ideal blackbody emits a similar amount of power within the two windows (Figure 1a), the primary window contributes to the majority of the cooling power. Moreover, the primary window is also less susceptible to water vapor[4,7] than the secondary window. As a result, extensive efforts have been devoted to the primary window, and different types of near-perfect infrared emitters were designed.[5] Various studies have shown that cooling power greater than 100W/m^2 can be achieved[6,8−11] and that the reported cooling power still keeps increasing in recent years. Therefore, it is about time to estimate the ultimate cooling ability of this technique and put forward a theoretical limit for further reference. To do that, the secondary window, which is globally available (Figure S1), must be included as it may provide an additional cooling power of more than 20 W/m^2.[4]

In this work, we calculated the theoretical limit of the radiative cooling power, taking into account both atmospheric windows. The transmittance data of the atmosphere is generated using the ATRAN modeling software in the 2−28 μm range.[12] In addition, we also proposed a possible approach, i.e., exploiting the localized surface plasmon resonance (LSPR) to reach the theoretical limit. The semiconductor nanoparticles (NPs) with appropriate carrier concentration generates LSPR in the mid-infrared region. This resonance arises from the resonant interaction of free charge carriers with the oscillating electromagnetic field and results in significant absorption enhancement near the resonance.[13−18] More importantly, the resonance peak is much wider than the molecular and phonon resonances,[9,10,19−23] which are widely exploited in current

Received: April 3, 2020
Revised: August 25, 2020
Published: August 26, 2020

https://dx.doi.org/10.1021/acs.nanolett.0c01457
Nano Lett. 2020, 20, 6974−6980

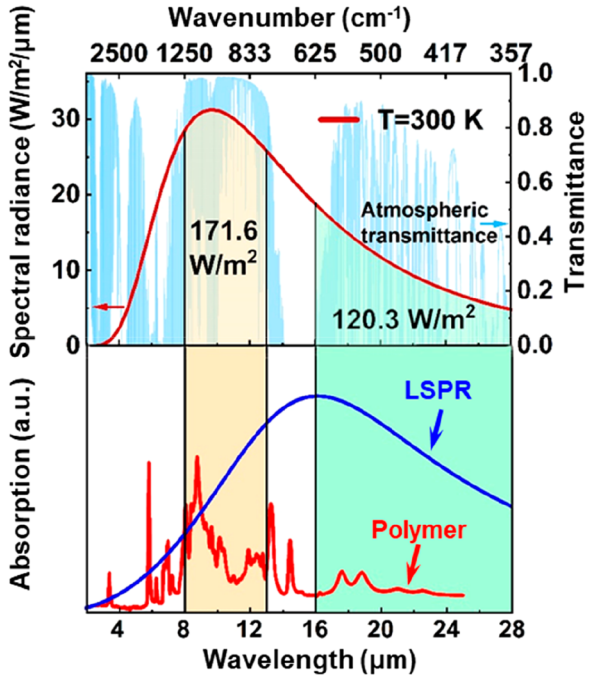

Figure 1. (a) Thermal radiation of a blackbody at room temperature and the atmospheric transmittance in the range of 2−28 μm. The power in the shaded area is the power emitted from a blackbody (b) IR absorption spectrum of PMMA (red line). The calculated IR absorption spectrum of metal oxide nanoparticles (blue line) arising from LSPR (Section III, Supporting Information for details).

literature (Figure 1b). Therefore, it has the potential to cover both atmospheric windows, which is very hard with current techniques unless some sophisticated photonic structures are adopted.[8,11,23−27] Meanwhile, by choosing wide band gap semiconductors, high solar transparency may also be achieved, which is almost impossible for other types of infrared emitters covering both windows.[28,29] To verify the cooling ability of this approach, we experimentally showed that adding self-doped indium oxide (In_2O_3) nanoparticles into poly(methyl methacrylate) (PMMA) significantly enhanced the emissivity in both windows. The net cooling power of the composite film at night is found to be close to the theoretical limit with the closest one only about 0.4 W/m^2 below the limit.

To obtain the theoretical limit of the radiative cooling power, we first studied the heat transfer balance, and the net cooling power P_{cool} is defined as

$$P_{cool}(T, T_a) = P_{rad}(T) - P_{atm}(T_a) - P_s - P_{nrad}(T, T_a) \quad (1)$$

T and T_a are temperatures of the surface and ambient air, respectively. $P_{rad}(T)$ is the power emitted per unit surface area, which increases with T. $P_{atm}(T_a)$ is the absorbed emission from the ambient air by the surface. P_s is the absorbed solar radiation, and $P_{nrad}(T,T_a)$ accounts for the nonradiative heat transfer and is interpreted as $h_c(T_a - T)$ by introducing a nonradiative heat transfer coefficient h_c (W/m^2/K). Under a certain ambient temperature, the surface temperature T drops for positive P_{cool}, and a steady state is achieved when P_{cool} becomes zero. It is natural to pick the temperature difference under the steady state; i.e., $\Delta T = T_a - T$ as the parameter to characterize the cooling ability of a device. However, depending on the real operating conditions, h_c may vary in a range of 2−20 W/m^2/K[25] so that ΔT can be quite different even for the same device under different ambient conditions. Therefore, to evaluate the cooling ability of different devices, a better parameter will be the cooling power, which can be experimentally measured with a heater to compensate for the heat loss due to thermal radiation.[11] During the measurement, the surface temperature T is kept the same as the ambient temperature T_a, and the nonradiative heat transfer power P_{nrad} becomes zero. The cooling power $P_{cooling}(T_a)$ is defined as $P_{cool}(T = T_a)$ and is equal to the power flowing from the heater to the device.

To obtain the theoretical limit of the cooling power, one can assume a complete reflection of solar energy, i.e., $P_s = 0$ and maximize the term $P_{rad}(T_a) - P_{atm}(T_a)$ as shown in eq 1. As a result[30]

$$P_{cooling}(T_a) = 2\pi \int_0^{\pi/2} \cos\theta \sin\theta \int_0^{\infty} I_b(T_a, \lambda) \varepsilon(\lambda, \theta)[1 - \varepsilon_a(\lambda, \theta)] d\lambda d\theta \quad (2)$$

in which $\varepsilon(\lambda,\theta)$ and $\varepsilon_a(\lambda,\theta)$ are the angular and spectral emissivity of the surface and the ambient air, respectively, θ is the zenith angle, and λ is the wavelength. $I_b(T,\lambda)$ is the spectral radiance of a blackbody at temperature T and follows Planck's law:

$$I_b(T, \lambda) = \frac{2\hbar c^2}{\lambda^5} \frac{1}{e^{\hbar c/\lambda k_B T} - 1} \quad (3)$$

$\hbar$ is Planck's constant, c is the speed of light, and k_B is the Boltzmann constant. The angular air emissivity $\varepsilon_a(\lambda,\theta)$ is defined as

$$\varepsilon_a(\lambda, \theta) = 1 - t_a(\lambda, 0)^{1/\cos\theta} \quad (4)$$

where $t_a(\lambda,0)$ is the spectra transmittance of the atmosphere at the zero zenith angle, and we used the data provided by the ATRAN modeling software in the wavelength range of 2−28 μm covering both windows.[12] The water vapor column is set as 1.0 mm to maximize the transparency of the secondary window (16−28 μm). Equation 2 clearly indicates that a perfect blackbody with $\varepsilon(\lambda,\theta) = 1$ reaches the maximum cooling power. Therefore, we set $\varepsilon(\lambda,\theta) = 1$ for calculating the limit. It is worth noting that a selective emitter that emits strongly only in the 8−13 μm primary window is typically regarded to be better than the blackbody emitter we adopted here.[19,31] However, if the secondary window is included, the power emitted via this window may outweigh the power absorbed from the atmosphere. In most common applications, when the temperature drop is around 10 K, the blackbody emitter is better than or at least as good as a selective emitter (Figure S2). In applications to achieve deep subfreezing temperatures,[19] a selective emitter is absolutely needed.

The calculated theoretical limit $P_{cooling}$ is illustrated in Figure 2 (blue circles). To clearly demonstrate the contributions from different windows, we also showed the achievable cooling power solely relying on the primary 8−13 μm window (violet circles). It becomes clear that the secondary window contributes about 20−40 W/m^2 of the total power. On the basis of the calculated data, we also obtained an empirical relation for the theoretical limit as follows:

$$P_{cooling} = \varepsilon\sigma(T_a - T_0)^4 \quad (5)$$

where $\sigma = 5.67 \times 10^{-8}$ W/m^2/K^4 is the Stefan−Boltzmann constant. $\varepsilon = 0.61$ and $T_0 = 34.5$ K were found with a least-square fit. Meanwhile, the cooling power due to the primary

https://dx.doi.org/10.1021/acs.nanolett.0c01457
Nano Lett. 2020, 20, 6974−6980

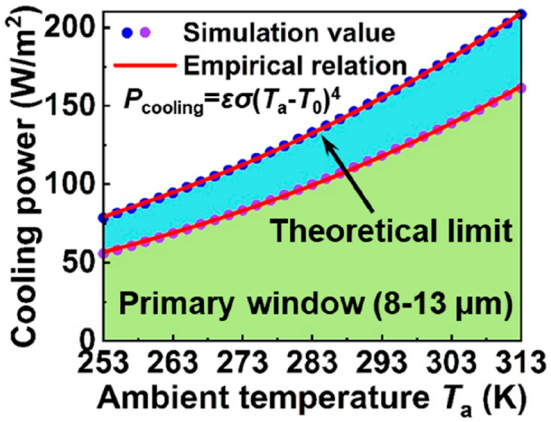

Figure 2. Theoretical limit of radiative cooling power. The blue and violet circles are simulation results of the whole window and the primary window, respectively. The solid curves are the least-squares fitting results with the empirical relation.

window also follows the same relation with the two parameters as $\varepsilon = 0.63$ and $T_0 = 53.4$ K, respectively. It can be regarded as the limit for a perfect selective emitter, which emits strongly only in the primary window.

In practical applications, covering both windows is not easy as the total width of the atmospheric window [1250 cm^{-1} (8 μm) − 357 cm^{-1} (28 μm) = 893 cm^{-1}] is much greater than the typical width (less than 50 cm^{-1}) of a molecular vibrational peak of polymer.[32] Here, we propose to exploit the LSPR of doped semiconductors to achieve strong radiations in both windows. The width of a resonance peak is close to the damping coefficient of the charge carrier. The typical carrier mobility μ in doped semiconductors for mid-infrared LSPR is about 20 $cm^2/V/s$.[16,17] The damping coefficient $\gamma = e/(m\mu)$ (e the elementary charge and m the effective electron mass taken as half of the free electron mass) is estimated to be around 900 cm^{-1}, which is comparable with the width of the atmospheric window. In reality, there might be other factors affecting the resonant peak, e.g., surface scattering,[33] mixing with lattice mode.[34] As will be shown below, our particle size is greater than the electron free path length (<10 nm) so that the surface scattering is negligible.[35] Meanwhile, the random distribution of nanoparticles at a relatively low concentration leads to the absence of lattice mode.

To demonstrate this idea, we use self-doped indium oxide (In_2O_3) to generate LSPR. In_2O_3 is a wide band gap semiconductor with high solar transparency (Figure S8), and adding In_2O_3 to the polymer film does not lead to an obvious rise of solar absorption (Figure S8). The In_2O_3 nanoparticles were synthesized via a simple one-step liquid phase method[36] (Section VI, Supporting Information). As shown in Figure 3a,b, we successfully obtained In_2O_3 NPs with diameters around 28 nm, and the X-ray diffraction pattern indicates a pure cubic bixbyite structure. The In_2O_3 NPs were dispersed in CCl_4 for FTIR measurement. As illustrated by Figure 3c, a wide LSPR peak shows up near 8 μm. Since no aliovalent element was added to replace In atoms during the synthesis, the LSPR must arise from the self-doping defects due to the presence of oxygen vacancy. The existence of oxygen vacancy was confirmed by X-ray photoelectron spectroscopy (XPS). Figure 3d is the O 1s core-level spectrum that can be deconvoluted into two distinct peaks. The peak at 530.79 eV corresponds to the oxygen bond of In−O−In, and the other peak at 532.31 eV is deemed as the oxygen defects.[37,38] We also further quantify the permittivity of the synthesized In_2O_3 with the help of the Drude model:

$$\varepsilon_p(f) = \varepsilon_\infty - \frac{f_p^2}{f(f + i\gamma)} \tag{6}$$

f is the frequency of light, $\varepsilon_\infty = 3.8$[17] is the high-frequency permittivity, f_p is plasma frequency, and γ is the damping coefficient. f, f_p, and γ are all in units of cm^{-1}. By fitting the FTIR data (Section III, Supporting Information), f_p and γ were extracted as 2900 and 1200 cm^{-1}, respectively. The damping coefficient γ is greater than the width of the atmospheric

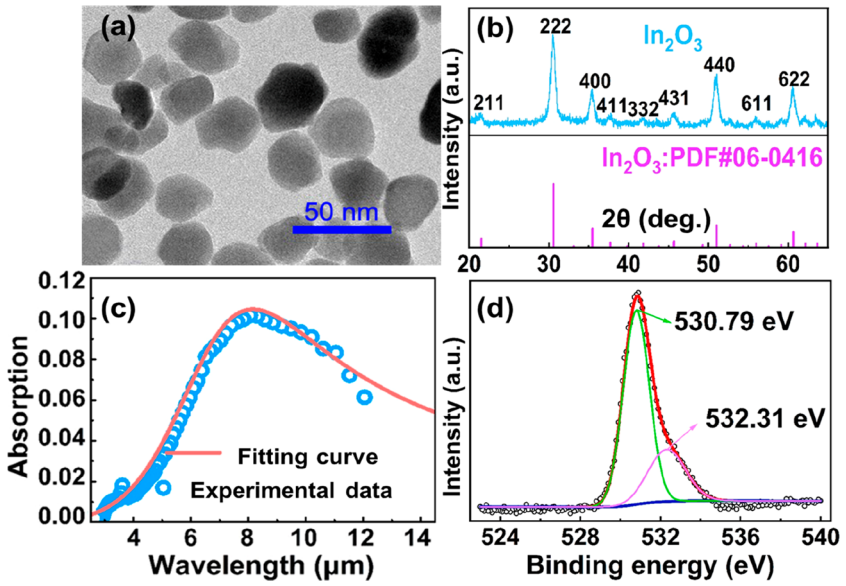

Figure 3. Characterizations of indium oxide Nps. (a) TEM image of In_2O_3. (b) XRD pattern of In_2O_3 Nps. (c) The measured FTIR spectrum of In_2O_3 Nps (blue circles) and the fitting results (red curve). (d) Curve fitting of the O 1s peak in the XPS spectrum of In_2O_3 Nps. Black circles are the experimental data, which are deconvoluted into two peaks centered at 530.79 eV (green curve) and 532.31 eV (pink curve).

https://dx.doi.org/10.1021/acs.nanolett.0c01457
Nano Lett. 2020, 20, 6974−6980

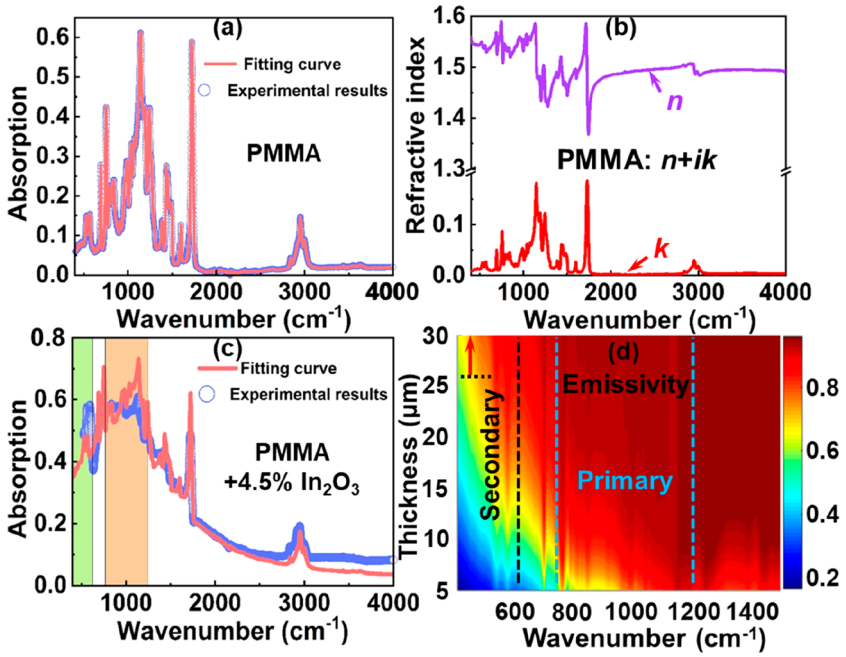

Figure 4. (a) The measured FTIR spectrum of PMMA film (blue circles) and the fitting results using the iterative algorithm (pink curve). (b) The real and imaginary part of the refractive index of PMMA extracted based on the experimental data. (c) The measured FTIR spectrum of the composite film (blue circles) and the fitting result using the Maxwell−Garnet model (pink curve). (d) The contour plot of spectral emissivity of a composite film of different thicknesses at zero zenith angle.

window (893 cm^{-1}), showing its potential to cover both windows. It is worth noting that all of the FTIR data in this work was obtained under the attenuated total reflection (ATR) mode and was not exactly the same as the spectrum emissivity of the surface (Section II, Supporting Information).

Poly(methyl methacrylate) was chosen as the host material to fabricate composite films containing In_2O_3 nanoparticles. As will be shown later, the choice of polymer is actually quite casual as strong emissivity in both windows can be achieved solely relying on LSPR. We first prepared the pure PMMA film by the drop-casting method and characterized its infrared property. The FTIR spectrum is shown in Figure 4a, and the permittivity ε_h of PMMA was extracted with an algorithm proposed by Ohta and Ishida[39,40] (Section IV, Supporting Information). Figure 4b is the optical constants of PMMA that will be used for further simulation, and the absorption spectrum calculated with the extracted optical constants shows excellent agreement with the experimental data (Figure 4a).

To fabricate the composite films, we added the acetone suspension of In_2O_3 NPs to the anisole solution of PMMA and stirred for over 24 h. The mixture was then scraped onto the aluminum substrates for infrared characterization and cooling tests. The FITR spectrum of the composite film containing 4.5% vol In_2O_3 is shown in Figure 4c. By adding In_2O_3 nanoparticles, an obvious enhancement of absorption can be seen in both windows by comparing Figure 4a and Figure 4c.

The emissivity of the composite film depends on the film thickness d and particle concentration χ. To find the appropriate parameters for achieving strong emissivity in both windows, we used the optical theory to calculate the angular spectrum emissivity $\varepsilon(\lambda,\theta)$. The transfer matrix method was used to obtain the reflection coefficient $R(\lambda,\theta)$ of a film with thickness d,[41,42] and the spectrum emissivity $\varepsilon(\lambda,\theta)$ is defined as

$$\varepsilon(\lambda, \theta) = 1 - \frac{R^s(\lambda, \theta) + R^p(\lambda, \theta)}{2} \tag{7}$$

where R^s and R^p are the reflection coefficient of the s- and p-polarized waves and the formula for the reflection coefficients can be found with eqs S8, S9, and S11 in Supporting Information. The optical constants of the composite film are based on Maxwell−Garnet model:[43]

$$\frac{\varepsilon_{eff} - \varepsilon_m}{\varepsilon_{eff} + 2\varepsilon_m} = \chi \frac{\varepsilon_p - \varepsilon_m}{\varepsilon_p + 2\varepsilon_m} \tag{8}$$

ε_{eff} is the effective permittivity of the composite film. ε_p and ε_m are the permittivity of In_2O_3 NPs and PMMA, respectively, and both of them were extracted from the experimental data directly as described above. χ is the volume fraction of the NPs. Figure 4c shows a good agreement indicating that the model is sufficiently accurate to predict the spectrum emissivity (Other fits can be found in Figure S9.) The optimal concentration range was found to be 3%−5% vol (Figure S7). Figure 4d clearly indicates that, under a constant volume fraction of 4.5%, the film thickness must be greater than 25 μm to achieve large emissivity in both windows. Moreover, the calculation with other different polymers (polystyrene and poly(vinyl alcohol))[44] shows similar spectrum emissivity due to the strong broadband enhancement of LSPR (Figure S7). It supports our early claim that the polymer selection is quite causal, which offers us great freedom to pick polymers with higher solar transparency in the future.

Following the theoretical estimation, the volume fraction of NPs was set at 4.5%, and the film was fabricated to be thicker than 25 μm (28.9 ± 1.7 μm as shown in Figure S10). We made a series of cooling performance measurements in Nanjing, China, from December 2019 to January 2020. To avoid solar irradiance, the test was conducted at night. We used a foam box with good thermal insulation as the measuring device

https://dx.doi.org/10.1021/acs.nanolett.0c01457
Nano Lett. 2020, 20, 6974−6980

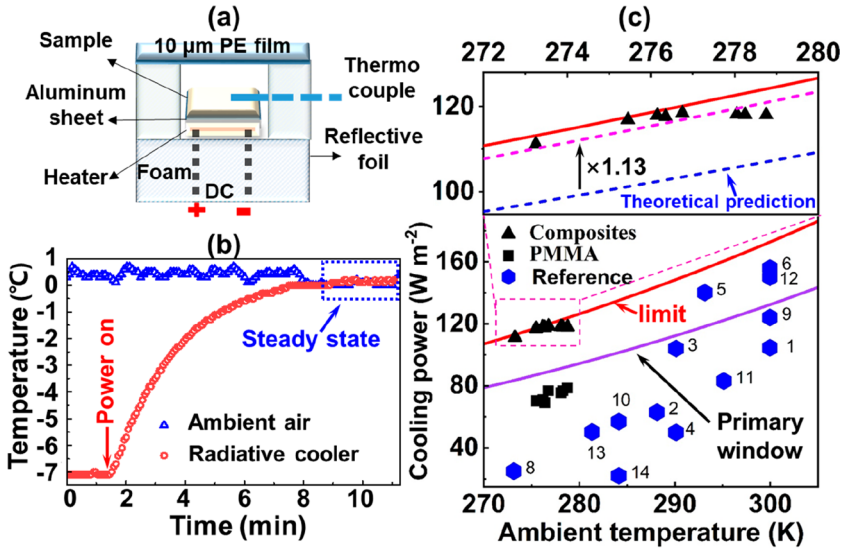

Figure 5. (a) Schematic of the radiative cooler testing device. (b) The ambient temperature and the composite surface temperature measured on December 31, 2019 in Nanjing, China. (c) The cooling power of composite film (black triangles) and pure PMMA (black square). The theoretical limit (red curve) and other reported results in the literatures (blue diamonds): (1) Zou et al.,[6] (2) Tian et al.,[45] (3) Bao et al.,[9] (4) A. R. Gentle et al.,[8] (5) Zhai et al.,[11] (6) Eden Rephaeli et al.,[27] (7) Nilsson et al.,[46] (8) Granqvist et al.,[47] (9) L. Ling et al.,[48] (10) B. Orel et al.,[49] (11) A. P. Raman et al.,[30] (12) Kou et al.,[20] (13) Hu et al.,[50] (14) D. Michell et al.[51]

(Figure 5a). The device was placed on an open roof of the building to ensure the direct emission into the sky. An electric heater was attached to the back of the radiative emitter and connected to a regulated DC power supply to keep the surface temperature the same as the ambient air (Figure 5a). The power supply was off initially, and a temperature drop of over 7 °C was achieved (Figure 5b). The power supply was then switched on, and the input power was adjusted to bring the whole system to a new steady state. We collected a series of cooling power data for the composite film at different ambient temperatures, and the pure PMMA film was also tested. An obvious increase of cooling power can be observed by adding In_2O_3(Figure 5c), and the cooling power of the composite film is extremely close to the limit with the closest value only about 0.4 W/m^2 below the limit. Our values appeared to be closer to the theoretical limit as compared to the reported data in the literature. For those cooling powers measured under daytime operations, we added the absorbed solar power to the total cooling power for comparison.

Meanwhile, the close-up image in Figure 5c showed that the measured values are only slightly higher than the theoretically predicted values, which is obtained by substituting eq 7 into eq 2. The parameters were set as χ = 4.5%, d = 28.9 μm, and the calculation did not involve any fitting parameters! The nice agreement between theory and experiment further consolidates the idea of plasmon-enhanced emissivity. The slightly higher experimental value is probably due to the surface roughness of the fabricated film (28.9 ± 1.7 μm Figure S10), which effectively increases the surface area, while a smooth surface was assumed in the simulation. To the best of our knowledge, this is the first experimental demonstration of LSPR enhancement on the radiative cooling ability. To achieve efficient daytime radiative cooling, one needs to select polymers with higher solar transparency and substrate with higher solar reflectance to suppress solar absorption as much as possible.

In summary, we calculated the theoretical limit of the cooling power of a radiative cooling device and put forward an empirical relation between the cooling power and ambient temperature. The theoretical limit may be treated as a standard to evaluate the performance of a device. Furthermore, we proposed and verified that one can approach this limit by exploiting the broadband LSPR enhancement of emissivity. The measured cooling power is very close to the limit indicating strong emissivity in both atmospheric windows. We hope that this work may pave the way for achieving even higher radiative cooling powers during the daytime operations with the help of LSPR.

■ ASSOCIATED CONTENT

Supporting Information

The Supporting Information is available free of charge at https://pubs.acs.org/doi/10.1021/acs.nanolett.0c01457.

Synthesis of In_2O_3 nanoparticle; fabrication of composite film; material characterizations; effect of latitude on radiation cooling; comparison of theoretical cooling performance between blackbody and selective emitters; cooling power calculated for different emissivity in the 13−16 μm band; the attenuated total reflection (ATR) mode of FTIR; Drude model and LSPR of In_2O_3 nanoparticle; algorithm to extract the optical constants of PMMA; optical theory to calculate the angular spectrum emissivity; the spectrum emissivity of pure polymer film and composite film (PDF)

■ AUTHOR INFORMATION

Corresponding Authors

Lin Wang − *State Key Laboratory of Infrared Physics, Shanghai Institute of Technical Physics, Chinese Academy of Sciences, Shanghai 200083, China*; Email: wanglin@mail.sitp.ac.cn

Yu Gu − *Key Laboratory of Advanced Display Materials and Devices, Ministry of Industry and Information Technology, Institute of Optoelectronics & Nanomaterials, College of Material Science and Engineering, Nanjing University of Science and Technology, Nanjing 210094, China*; orcid.org/0000-0003-1793-7409; Email: yug@njust.edu.cn

https://dx.doi.org/10.1021/acs.nanolett.0c01457
Nano Lett. 2020, 20, 6974−6980

Authors

Rongkang Zhu − *Key Laboratory of Advanced Display Materials and Devices, Ministry of Industry and Information Technology, Institute of Optoelectronics & Nanomaterials, College of Material Science and Engineering, Nanjing University of Science and Technology, Nanjing 210094, China*

Dawei Hu − *Key Laboratory of Advanced Display Materials and Devices, Ministry of Industry and Information Technology, Institute of Optoelectronics & Nanomaterials, College of Material Science and Engineering, Nanjing University of Science and Technology, Nanjing 210094, China*

Zhi Chen − *College of Civil Science and Engineering, Yangzhou University, Yangzhou 225127, China*

Xiaobao Xu − *Key Laboratory of Advanced Display Materials and Devices, Ministry of Industry and Information Technology, Institute of Optoelectronics & Nanomaterials, College of Material Science and Engineering, Nanjing University of Science and Technology, Nanjing 210094, China*

Yousheng Zou − *Key Laboratory of Advanced Display Materials and Devices, Ministry of Industry and Information Technology, Institute of Optoelectronics & Nanomaterials, College of Material Science and Engineering, Nanjing University of Science and Technology, Nanjing 210094, China;* orcid.org/0000-0001-5834-5579

Complete contact information is available at: https://pubs.acs.org/10.1021/acs.nanolett.0c01457

Author Contributions

R.Z., D.H., and Z.C. contributed equally. The manuscript was written through contributions of all authors. All authors have given approval to the final version of the manuscript.

Notes

The authors declare no competing financial interest.

■ ACKNOWLEDGMENTS

This work was financially supported by the National Key R&D Program of China (2017YFA0305500), the National Science Foundation of China (11604152), the Natural Science Foundation of Jiangsu Province (SBK2020030142, BK20160815, BK20181079, and BK20190443), and the Fundamental Research Funds for the Central Universities (30919011298 and 30919011299)

■ REFERENCES

(1) Lin, W.; Ma, A.; Zhou, X.; Tan, Y.; Yan, X.; Yu, W. *Environment and Energy Challenge of Air Conditioner in China, International Conference on Bioinformatics & Biomedical Engineering*; IEEEChina: China, 2008; pp 4413−4416.

(2) Santamouris, M.; Feng, J. Recent progress in daytime radiative cooling: Is it the air conditioner of the future? *Buildings* **2018**, *8* (12), 168.

(3) Family, R.; Mengüç, M. P. Materials for Radiative Cooling: A Review. *Procedia Environ. Sci.* **2017**, *38*, 752−759.

(4) Sun, X.; Sun, Y.; Zhou, Z.; Alam, M. A.; Bermel, P. Radiative sky cooling: fundamental physics, materials, structures, and applications. *Nanophotonics* **2017**, *6* (5), 997−1015.

(5) Zeyghami, M.; Goswami, D. Y.; Stefanakos, E. A review of clear sky radiative cooling developments and applications in renewable power systems and passive building cooling. *Sol. Energy Mater. Sol. Cells* **2018**, *178*, 115−128.

(6) Zou, C.; Ren, G.; Hossain, M. M.; Nirantar, S.; Withayachumnankul, W.; Ahmed, T.; Bhaskaran, M.; Sriram, S.; Gu, M.; Fumeaux, C. Metal-Loaded Dielectric Resonator Metasurfaces for Radiative Cooling. *Adv. Opt. Mater.* **2017**, *5* (20), 1700460.

(7) Idso, S. B.; Jackson, R. D. Thermal radiation from the atmosphere. *Journal of Geophysical Research* **1969**, *74* (23), 5397−5403.

(8) Gentle, A. R.; Smith, G. B. Radiative heat pumping from the Earth using surface phonon resonant nanoparticles. *Nano Lett.* **2010**, *10* (2), 373−9.

(9) Bao, H.; Yan, C.; Wang, B.; Fang, X.; Zhao, C. Y.; Ruan, X. Double-layer nanoparticle-based coatings for efficient terrestrial radiative cooling. *Sol. Energy Mater. Sol. Cells* **2017**, *168*, 78−84.

(10) Huang, Z.; Ruan, X. Nanoparticle embedded double-layer coating for daytime radiative cooling. *Int. J. Heat Mass Transfer* **2017**, *104*, 890−896.

(11) Zhai, Y.; Ma, Y.; David, S. N.; Zhao, D.; Lou, R.; Tan, G.; Yang, R.; Yin, X. Scalable-manufactured randomized glass-polymer hybrid metamaterial for daytime radiative cooling. *Science* **2017**, *355*, 1062.

(12) Lord, S. D. A new software tool for computing Earth's atmospheric transmission of near- and far-infrared radiation. In *NASA Technical Memorandum 103957*, 1992.

(13) Maier, S. A. *Plasmonics: Fundamentals and Applications*; Springer: New York, 2007.

(14) Liu, X.; Swihart, M. T. Heavily-doped colloidal semiconductor and metal oxide nanocrystals: an emerging new class of plasmonic nanomaterials. *Chem. Soc. Rev.* **2014**, *43* (11), 3908−20.

(15) Agrawal, A.; Cho, S. H.; Zandi, O.; Ghosh, S.; Johns, R. W.; Milliron, D. J. Localized surface plasmon resonance in semiconductor nanocrystals. *Chem. Rev.* **2018**, *118* (6), 3121−3207.

(16) Gu, Y.; Li, X. M.; Chen, J.; Zeng, H. B. Anomalous plasmon resonance from confined diffusive charges: high quality and tunability from mid to far infrared wavebands. *Opt. Express* **2016**, *24* (26), 29908−29921.

(17) Gu, Y.; Zhu, Z. F.; Song, J. Z.; Zeng, H. B. Triangle-, tripod-, and tetrapod-branched ITO nanocrystals for anisotropic infrared plasmonics. *Nanoscale* **2017**, *9* (48), 19374−19383.

(18) Gu, Y.; Chen, Z.; Chen, L. Designing a broadband terahertz plasmonic field enhancer with a homojunction of semiconductors. *Appl. Phys. Express* **2020**, *13* (1), 012005.

(19) Chen, Z.; Zhu, L.; Raman, A.; Fan, S. Radiative cooling to deep sub-freezing temperatures through a 24-h day-night cycle. *Nat. Commun.* **2016**, *7*, 13729.

(20) Kou, J.-l.; Jurado, Z.; Chen, Z.; Fan, S.; Minnich, A. J. Daytime Radiative Cooling Using Near-Black Infrared Emitters. *ACS Photonics* **2017**, *4* (3), 626−630.

(21) Mandal, J.; Fu, Y.; Overvig, A. C.; Jia, M.; Sun, K.; Shi, N. N.; Zhou, H.; Xiao, X.; Yu, N.; Yang, Y. Hierarchically porous polymer coatings for highly efficient passive daytime radiative cooling. *Science (Washington, DC, U. S.)* **2018**, *362* (6412), 315−319.

(22) Leroy, A.; Bhatia, B.; Kelsall, C. C.; Castillejo-Cuberos, A.; Di Capua, H. M.; Zhao, L.; Zhang, L.; Guzman, A. M.; Wang, E. N. High-performance subambient radiative cooling enabled by optically selective and thermally insulating polyethylene aerogel. *Science advances* **2019**, *5* (10), eaat9480.

(23) Gentle, A. R.; Smith, G. B. A Subambient Open Roof Surface under the Mid-Summer Sun. *Adv. Sci. (Weinh)* **2015**, *2* (9), 1500119.

(24) Hossain, M. M.; Jia, B.; Gu, M. A Metamaterial Emitter for Highly Efficient Radiative Cooling. *Adv. Opt. Mater.* **2015**, *3* (8), 1047−1051.

(25) Tian, Y.; Qian, L.; Liu, X.; Ghanekar, A.; Xiao, G.; Zheng, Y. Highly effective photon-to-cooling thermal device. *Sci. Rep.* **2019**, *9* (1), 19317.

(26) Zhou, L.; Song, H.; Liang, J.; Singer, M.; Zhou, M.; Stegenburgs, E.; Zhang, N.; Xu, C.; Ng, T.; Yu, Z.; Ooi, B.; Gan, Q. A polydimethylsiloxane-coated metal structure for all-day radiative cooling. *Nature Sustainability* **2019**, *2* (8), 718−724.

(27) Rephaeli, E.; Raman, A.; Fan, S. Ultrabroadband photonic structures to achieve high-performance daytime radiative cooling. *Nano Lett.* **2013**, *13* (4), 1457−61.

(28) Cooper, T. A.; Zandavi, S. H.; Ni, G. W.; Tsurimaki, Y.; Huang, Y.; Boriskina, S. V.; Chen, G. Contactless steam generation and superheating under one sun illumination. *Nat. Commun.* **2018**, *9*, 1.
(29) Menon, A. K.; Haechler, I.; Kaur, S.; Lubner, S.; Prasher, R. S. Enhanced solar evaporation using a photo-thermal umbrella for wastewater management. *Nature Sustainability* **2020**, *3* (2), 144.
(30) Raman, A. P.; Anoma, M. A.; Zhu, L.; Rephaeli, E.; Fan, S. Passive radiative cooling below ambient air temperature under direct sunlight. *Nature* **2014**, *515* (7528), 540−4.
(31) Zhao, D.; Aili, A.; Zhai, Y.; Xu, S.; Tan, G.; Yin, X.; Yang, R. Radiative sky cooling: Fundamental principles, materials, and applications. *Appl. Phys. Rev.* **2019**, *6* (2), No. 021306.
(32) Tsuda, S.; Yamaguchi, S.; Kanamori, Y.; Yugami, H. Spectral and angular shaping of infrared radiation in a polymer resonator with molecular vibrational modes. *Opt. Express* **2018**, *26* (6), 6899−6915.
(33) Hartland, G. V. Optical Studies of Dynamics in Noble Metal Nanostructures. *Chem. Rev.* **2011**, *111* (6), 3858−3887.
(34) Teperik, T. V.; Degiron, A. Design strategies to tailor the narrow plasmon-photonic resonances in arrays of metallic nanoparticles. *Phys. Rev. B: Condens. Matter Mater. Phys.* **2012**, *86* (24), 1.
(35) Matsui, H.; Furuta, S.; Tabata, H. Role of electron carriers on local surface plasmon resonances in doped oxide semiconductor nanocrystals. *Appl. Phys. Lett.* **2014**, *104* (21), 211903.
(36) Kanehara, M.; Koike, H.; Yoshinaga, T.; Teranishi, T. Indium Tin Oxide Nanoparticles with Compositionally Tunable Surface Plasmon Resonance Frequencies in the Near-IR Region. *J. Am. Chem. Soc.* **2009**, *131* (49), 17736−17737.
(37) Gan, J.; Lu, X.; Wu, J.; Xie, S.; Zhai, T.; Yu, M.; Zhang, Z.; Mao, Y.; Wang, S. C.; Shen, Y.; Tong, Y. Oxygen vacancies promoting photoelectrochemical performance of In(2)O(3) nanocubes. *Sci. Rep.* **2013**, *3*, 1021.
(38) Qi, Y.; Song, L.; Ouyang, S.; Liang, X.; Ning, S.; Zhang, Q.; Ye, J. Photoinduced Defect Engineering: Enhanced Photothermal Catalytic Performance of 2D Black In2 O3- x Nanosheets with Bifunctional Oxygen Vacancies. *Adv. Mater.* **2020**, *32*, No. 1903915.
(39) Ohta, K.; Ishida, H. Comparison Among Several Numerical Integration Methods for Kramers-Kronig Transformation. *Appl. Spectrosc.* **1988**, *42* (6), 952−957.
(40) Ohta, K.; Ishida, H. Efficient method for optical constant determination by FTIR-ATR. *Proc. SPIE* **1991**, *1575*, 604−605.
(41) Katsidis, C. C.; Siapkas, D. I. General transfer-matrix method for optical multilayer systems with coherent, partially coherent, and incoherent interference. *Appl. Opt.* **2002**, *41* (19), 3978−3987.
(42) Mitsas, C. L.; Siapkas, D. I. Generalized matrix method for analysis of coherent and incoherent reflectance and transmittance of multilayer structures with rough surfaces, interfaces, and finite substrates. *Appl. Opt.* **1995**, *34* (10), 1678−1683.
(43) Cai, W.; Shalaev, V. M. *Optical metamaterials: fundamentals and applications*; Springer: New York, 2010; pp 12−200.
(44) Pacansky, J.; England, C.; Waltman, R. J. Complex refractive indexes for polymers over the infrared spectral region: Specular reflection IR spectra of polymers. *J. Polym. Sci., Part B: Polym. Phys.* **1987**, *25* (4), 901−933.
(45) Li, T.; Zhai, Y.; He, S.; Gan, W.; Wei, Z.; Heidarinejad, M.; Dalgo, D.; Mi, R.; Zhao, X.; Song, J.; Dai, J.; Chen, C.; Aili, A.; Vellore, A.; Martini, A.; Yang, R.; Srebric, J.; Yin, X.; Hu, L. A radiative cooling structural material. *Science (Washington, DC, U. S.)* **2019**, *364* (6442), 760.
(46) Nilsson, T. M.J.; Niklasson, G. A.; Granqvist, C. G. A solar reflecting material for radiative cooling applications: ZnS pigmented polyethylene. *Sol. Energy Mater. Sol. Cells* **1992**, *28* (2), 175−193.
(47) Granqvist, C. G.; Hjortsberg, A. Radiative cooling to low temperatures: General considerations and application to selectively emitting SiO films. *J. Appl. Phys.* **1981**, *52* (6), 4205−4220.
(48) Ling, L.; Zhu, R.; Gu, Y.; Chen, Z. Doped semiconductor nanoparticles for possible daytime radiative cooling applications. *Semicond. Sci. Technol.* **2020**, *35*, 075018.
(49) Orel, B.; Gunde, M. K.; Krainer, A. Radiative cooling efficiency of white pigmented paints. *Sol. Energy* **1993**, *50* (6), 477−482.
(50) Hu, M.; Pei, G.; Wang, Q.; Li, J.; Wang, Y.; Ji, J. Field test and preliminary analysis of a combined diurnal solar heating and nocturnal radiative cooling system. *Appl. Energy* **2016**, *179*, 899−908.
(51) Michell, D.; Biggs, K. L. Radiation cooling of buildings at night. *Appl. Energy* **1979**, *5* (4), 263−275.

https://dx.doi.org/10.1021/acs.nanolett.0c01457
Nano Lett. 2020, 20, 6974−6980